Korean J. Chem. Eng., 34(12), 3195-3199 (2017)
DOI: 10.1007/s11814-017-0226-7

pISSN: 0256-1115
eISSN: 1975-7220

Spherical graphene and Si nanoparticle composite particles for high-performance lithium batteries

Jaehyun Lee and Jun Hyuk Moon†

Department of Chemical and Biomolecular Engineering, Sogang University, Seoul 04107, Korea
(*Received 10 March 2017 • accepted 10 August 2017*)

Abstract−Silicon/carbon composite electrodes are in the spotlight as an anode with a high capacity and a long cycle life. For this purpose, it is important to make a uniformly dispersed composite material. We fabricated spherical composite particles of reduced graphene oxide (rGO) and silicon nanoparticle (Si NP) using a spray drying method. The composite microparticle fabricated by drying the suspended droplets forms a well-agglomerated rGO/Si NP composite and forms a pore structure by crumpled rGO. The rGO/Si NP microparticles were applied as the anode of the lithium-ion battery. We achieved a reversible capacity of 1,246 mAh/g at 1A/g after 200 charge/discharge cycles and a capacity retention of 83%. Considering that the Si NP microparticle without rGO showed a capacity of 365 mAh/g and a retention of 12%, the rGO matrix improves the electrical conductivity and effectively alleviates stress during charge and discharge cycles.

Keywords : Silicon Nanoparticles, Reduced Graphene Oxides, Lithium Ion Batteries

INTRODUCTION

The development of advanced lithium-ion batteries (LIBs) for energy storage in various types of electronic devices that require light weight, long life, high power and high energy density is a great challenge [1-4]. However, current LIBs have limited storage capacity, and thus, high capacity and high density LIB technology is needed to meet the growing demand for industrial applications [5,6] Si is attracting attention as an LIB anode due to its excellent theoretical capacity of 4,000 mAh/g, approximately 10 ten-times larger than conventional graphite anode [7]. However, Si undergoes large volume changes (>300%) during lithiation and delithiation processes, resulting in severe breakdown of the electrode and subsequent electrical disconnection, and thus, a significant capacity drop [8]. Extensive research has addressed these issues using Si nanostructures, including nanowires [9,10], nanotubes [11-13], nanoparticles, porous structures [14,15] and composites with carbon materials.

Graphene is a single layer carbon sheet with sp^2-hybridized carbon lattice. Graphene is known to have excellent electronic conductivity, excellent mechanical flexibility, excellent chemical stability and high specific area [16,17]. Graphene and Si composites have been studied extensively as LIB electrodes [18-20]. This composite electrode could accommodate the volume changes of Si due to the excellent physical properties of graphene and improve the conductivity of the electrode, thus enabling high capacity and cycle retention [21]. For example, Zhu et al. fabricated Si/graphene composites through self-assembly of NH_2-terminal Si nanowires and graphene oxide (GO) with high capacity retention of 1,335 mAh/g after 80 cycles at 0.2 A/g [22]. Zhou et al. assembled Si nanoparticles and surface modified graphene with poly(diallydimethylammonium chloride). This composite electrode showed a reversible capacity of 1,205 mAh/g over 150 cycles at 0.1 A/g [23]. Liu et al. designed a sandwich nanoarchitecture of rolled Si/reduced graphene oxide (rGO) bilayer. This composite showed a high capacity of 821 mAh/g after 700 cycles at 1 A/g [24]. Gao et al. synthesized a multilayer structure of Si/rGO through inexpensive electroless etching and graphene self-encapsulating approach. They exhibited a reversible capacity of 1,026 mAh/g over 50 cycles at 1 A/g [25]. However, because 2D graphene composites tend to be reconstructed through π-π interactions in the synthesis process, the resulting composite material reduces the available surface area due to limited electron and ion transport [26]. Recent research has suggested various methods to maintain the inherent characteristics of individual graphene sheets [27,28]. The crumpled graphene or encapsulated graphene and Si composite did not sacrifice the physical properties of graphene [29-31].

In this study, spherical particles of Si nanoparticle and graphene composites were prepared by using spray drying. Unlike typical film morphology, with spherical morphology it is easy to make high concentration dispersions, and consequently, it is easy to form thick electrodes for high energy density [20,21]. Rapid drying by spray drying makes it possible to mass-produce composite particles. Briefly, fine droplets of GO and Si nanoparticles were formed and dried, and spherical microparticles of rGO/Si NP composites were produced by thermal reduction of graphene oxide. In particular, when dried inside a droplet, the GO flakes are crumpled and thus, do not get aggregated, forming spherical particles containing pores in which Si nanoparticles are well dispersed. The lithium ion battery of rGO/Si NP microsphere anode exhibited a reversible capacity of

†To whom correspondence should be addressed.
E-mail: junhyuk@sogang.ac.kr
‡This article is dedicated to Prof. Kipung Yoo on the occasion of his retirement from Sogang University.

1,246 mAh/g at 1 A/g after 200 charge/discharge cycles. In contrast, Si microsphere cells showed a capacity of 365 mAh/g. In addition, the capacity retention rate was 83% for rGO/Si NP microparticles and only 12% for Si microparticles. This indicates that the rGO effectively buffers the volumetric change that is attributed to Si lithiation/delithiation, and also provides a good electrical conductive matrix.

EXPERIMENTAL SECTION

1. Synthesis of rGO/Si NP Microparticles

GO (Graphene Supermarket) and Si NPs (Sigma Aldrich) were dispersed in water/ethanol (70 : 30 v/v%) mixture to obtain a stable Si-GO suspension. The size of Si NPs was measured by light scattering method, and Si NPs were approximately 100 nm in size in a solution of ethanol and water (see Fig. S1). We confirmed that the Si nanoparticles dispersed in the mixture of ethanol and water were retained for several days without precipitation by agglomeration (see Fig. S2). We obtained GO/Si microparticles by spray drying this solution. A spray dryer was used for the preparation of GO/Si microparticles. The spray drier was operated at a flow rate of spraying solution of 3 ml/min and a chamber temperature of 140 °C. We heat treated the sample at 700 °C in an Ar atmosphere. During this heat treatment, GO is reduced to rGO.

2. Material Characterization

The morphologies and microstructures of the samples were observed by scanning electron microscopy (SEM) (FESEM, Carl Zeiss, SUPRA 55VP) and energy-dispersive spectroscopy (EDX, BRUKER, XFlash Detector 4010) elemental mapping was performed to examine the spatial distribution of the prepared materials. High-resolution transmission electron microscopy (HRTEM) (JEM-3010, JEOL). Raman spectra were recorded using a Horiba Jobin Yvon LabRam HR equipped with an air-cooled Ar-ion laser operated at 514 nm. X-ray diffraction (XRD) patterns were obtained using a Davinci D8 Advance diffractometer using Cu-Kα radiation; the samples were scanned between 10 and 90° at a scan rate of 0.04°/s. Thermogravimetric analysis (TGA) was conducted by heating the sample to 800 °C in air at a heating rate of 4 °C/min (TA instrument TGA Q50).

3. Electrochemical Characterization

We fabricated an anode film by doctor blade coating a slurry containing 60 wt% of active material, 20 wt% of conductive agent (DB-100), and 20 wt% of poly (acrylic acid). The copper foil was used as the current collector of the anode electrode, and the areal mass density of the active material was approximately 1 mg cm^{-2}. CR2032 coin-type cells were assembled using rGO/Si NP microsphere electrode, Li-metal counter electrode and polypropylene membrane. A mixture solution of 1 M $LiPF_6$ dissolved in a mixture of ethylene carbonate (EC)/ethyl methyl carbonate (EMC)/dimethyl carbonate (DMC) was used as electrolyte solution. The battery performance was evaluated by using a Maccor 4300 test system. Electrochemical impedance analyses of cells were performed by electrochemical impedance spectroscopy (EIS) using an impedance analyzer (Versastat, AMETEK). The measurements were in the 1 MHz to 0.1 Hz frequency range with a voltage amplitude of 10 mV.

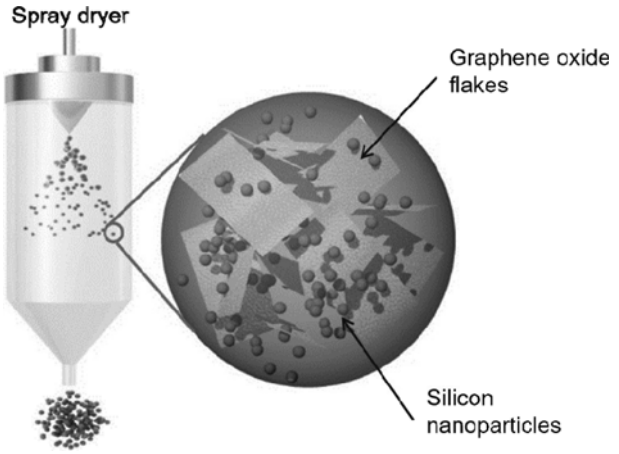

Scheme 1. Formation of GO/Si NP composite microparticles by spray drying.

RESULTS AND DISCUSSION

We briefly describe the fabrication of rGO/Si NP microparticles by spray drying, as shown in Scheme 1. We prepared a solution of GO and Si nanoparticles dispersed in a mixture of ethanol and water, and spray-dried the solution. Under high temperature drying condition (140 °C), the droplets of the sprayed dispersion rapidly dried to form GO/Si nanoparticle microparticles. In heat treatment at 700 °C and Ar atmosphere, GO was reduced to rGO to form rGO/Si NP microparticle. Figs. 1(a) and 1(b) are SEM images of rGO/Si NP microparticles. The size of the rGO/Si NP microparticles is uniform and the average diameter is about 5 μm. A crumpled rGO shell is observed on the surface, as observed in Fig. 1(c). Si nanoparticles are included between graphene layers. We believe that nanoparticles may be effective in preventing stacking of graphene flakes. Fig. 1(d) shows the cross-section of the microparticle. In the EDS mapping, a composite of Si and rGO can be found inside the microparticle.

The content of Si in rGO/Si NP microparticles was analyzed by TGA, as shown in Fig. 2(a). A large mass loss at 600 means decomposition of carbon, and the slight increase in mass at temperatures above 600 °C is due to oxidation of Si. As a result, the content of Si in the microparticle was about 63 wt%. The XRD peak of the rGO/Si NP microparticle is shown in Fig. 2(b). Bare Si microparticles (Si microparticles) were also fabricated by spray drying Si NP dispersion for comparison. Both results show the diffraction peaks at about 28.5°, 47.3° and 56.2°, which correspond to the (111), (220) and (311) planes of crystalline Si, respectively [15,32]. In the case of rGO/Si NP microparticles, they exhibit a wide peak at around 23°. This broad diffraction peak is attributed to the presence of rGO, which indicates that the graphene sheets are out of order in the lamination direction, and thus the composites are composed primarily of single or a few rGO layers [33]. Raman spectroscopic analysis of rGO/Si NP microparticles and bare Si microparticles was performed. The intense peak at 516 cm^{-1} represents crystalline Si (see Fig. 2(c)) [32,34]. The broad peaks at 1,350 cm^{-1} and 1,590 cm^{-1} are well-known characteristic peaks of graphite carbon. The former is due to disordered graphite (D mode), and the

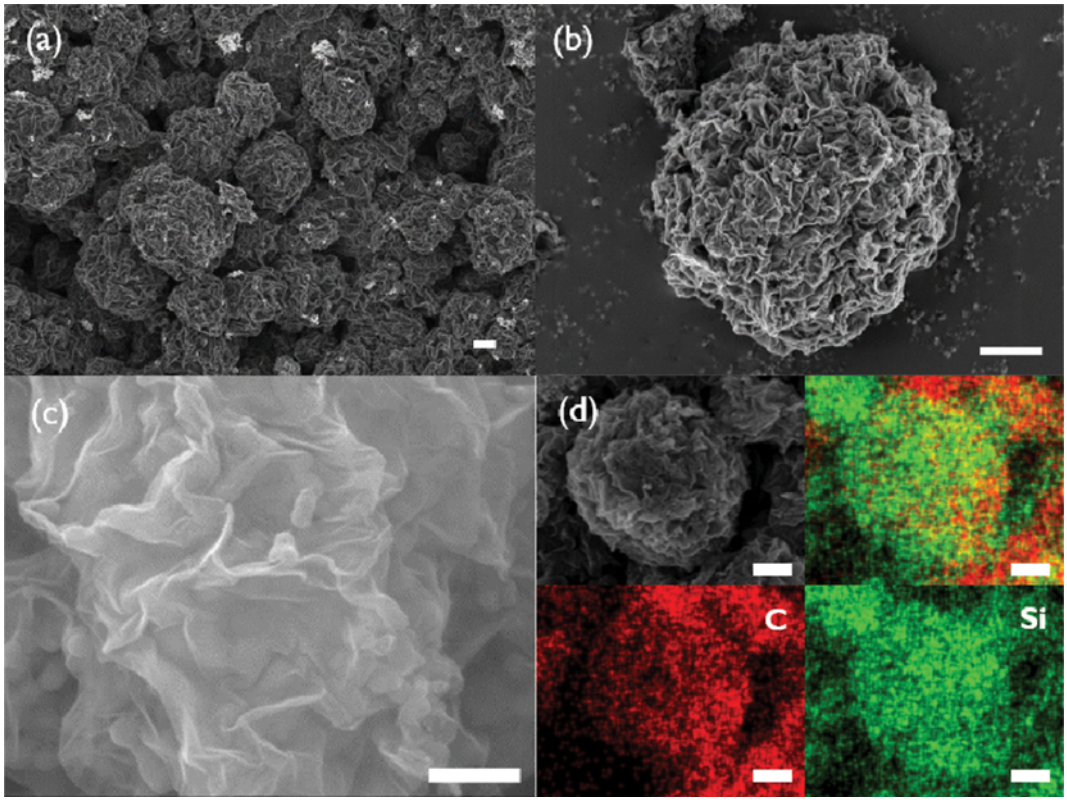

Fig. 1. SEM images of (a), (b) rGO/Si NP microparticles (scale bar: 1 μm) (c) High magnification SEM image of rGO/Si NP microparticles (scale bar: 200 nm) (d) Elemental mapping of rGO/Si NP microparticles (scale bar: 1 μm).

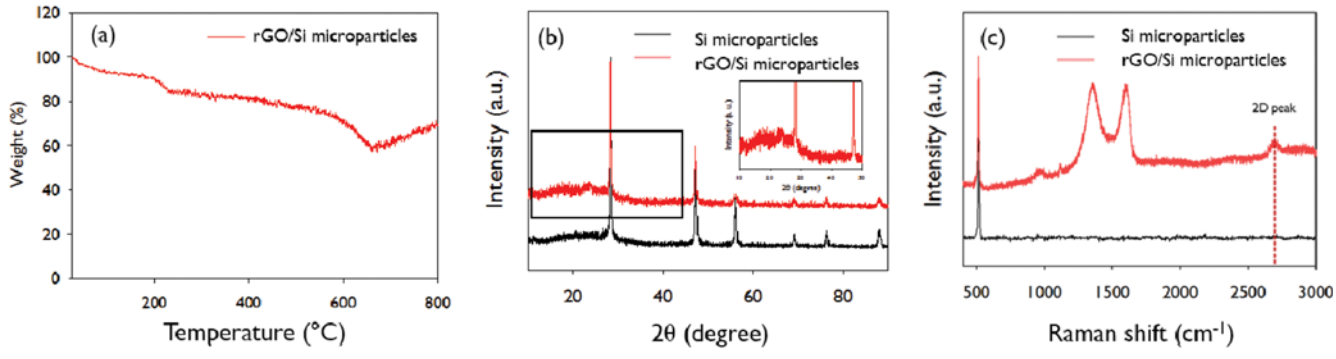

Fig. 2. (a) Thermogravimetric analysis curve of the rGO/Si NP microparticles in air. (b) XRD pattern and (c) Raman spectra of of Si microparticles and rGO/Si NP microparticles.

latter is due to scattering of vibration of sp^2 graphite carbon region (G mode) [35]. The peak ratio of D and G (I_D/I_G) is known as a parameter to evaluate the graphitization of carbon-based materials and the defect density of graphene materials. After heat reduction, the I_D/I_G ratio increased from 1.03 to 1.11 (see Fig. S3). This is due to the presence of local sp^3 defects in the sp^2 carbon network at the time of the detachment of the exfoliated GO [36]. We also identify the 2D of graphene at 2,700 cm^{-1} [37].

The electrochemical performance of rGO/Si NP microparticles was evaluated by assembling a coin cell LIB. The charge/discharge voltage profile of 1st cycle, 2nd cycle and 50th cycle is shown in Fig. 3(a). The profile was measured from a 0-2 V vs. Li/Li^+ voltage window at a current density of 1 A/g. The first discharge (lithiation) profile represents a potential step in the range of 0.7 to 0.3 V. This indicates the irreversible insertion of lithium ions into the Si nanoparticles (i.e., formation of an amorphous Li_xSi phase) while forming the SEI layer [15,38]. This profile then shows a long flat plateau starting at about 0.1 V, representing a crystalline Si Li alloy process [39]. The voltage of this plateau shifts to 0.4 V in the second cycle, which can be explained by the Li alloying with amorphous Si after the first cycle. In the first discharge, a stable SEI film was formed on the carbon surface, so a small plateau of 0.8 V disappeared after the first cycle [40].

The cycling capability of rGO/Si NP microparticles and Si mi-

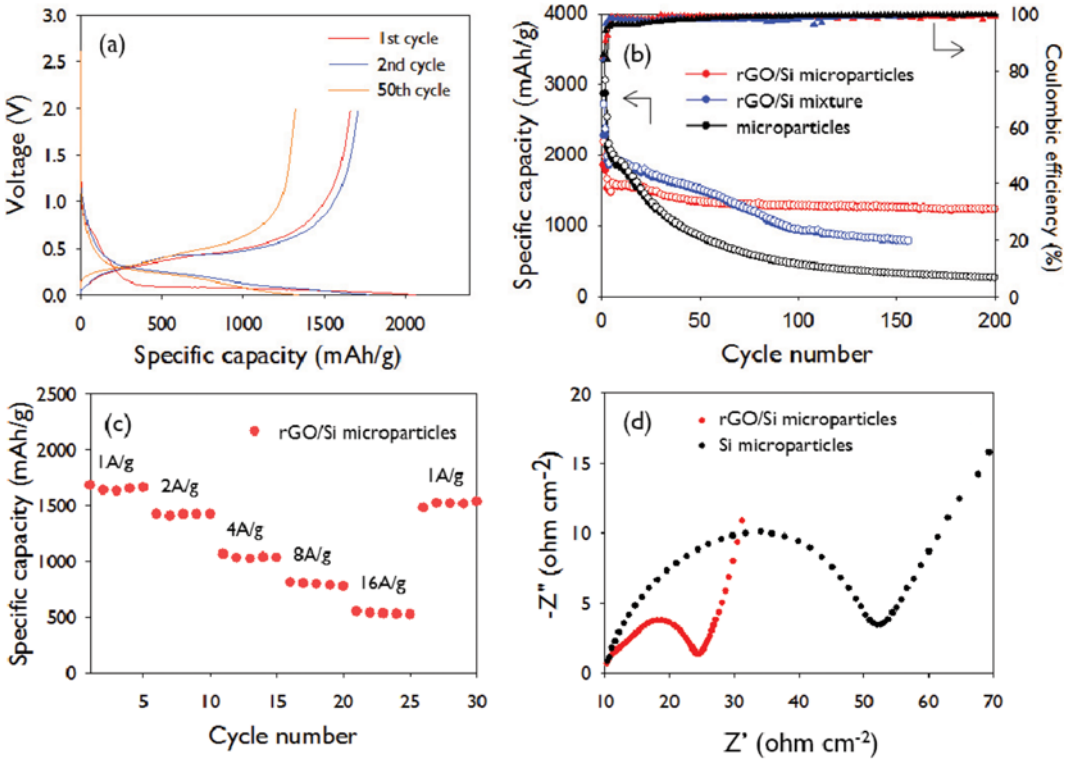

Fig. 3. (a) Charge/discharge voltage profile of rGO/Si NP microparticles. (b) Cycling performance and columbic efficiency of rGO/Si NP microparticle and Si microparticle electrodes at 1 A/g. (c) Rate capabilities of rGO/Si NP microparticles electrodes measured at various current densities from 1 to 16 A/g. (d) Impedance spectra measured after rate capability test of rGO/Si NP microparticles and Si microparticles.

croparticles was evaluated at 0-2 V versus Li/Li^+ voltage window at a rate of 1 A/g after initial two-cycle activation at 100 mA/g. The result is shown in Fig. 3(b). Here, RGO/Si mixture was obtained by drying the same dispersion at 60 °C for comparison. The specific capacity of the electrode was calculated based on the weight of the active material. The rGO/Si NP microparticles LIB exhibit a capacity of 2,290 mAh/g and 1,859 mAh/g for initial discharge and charge, respectively, with an initial columbic efficiency of 81%. The high irreversible capacity loss in the first cycle is due to volume change and pulverization of the electrode due to the formation of the SEI layer [24]. However, as shown in Fig. 3(b), The coulomb efficiency is restored to over 99% after the next four cycles. Meanwhile, the cycling ability of the Si microsphere and rGO/Si NP microsphere anode LIB was measured under the same condition. The Si microparticles LIB delivered an initial discharge capacity of 3,353 mAh/g, but sharply decreased to 365 mAh/g after 200 cycles. Therefore, after 200 cycles, the retention ratio was 12%. The capacity retention of rGO/Si NP microsphere anode LIB was 83% at 200 cycles. This result shows that the graphene assembled matrix effectively relieves mechanical stress due to large volume changes during lithiation/delithiation [41]. Moreover, the formation of rGO and Si composite electrodes by spray drying produces a more stable electrical conduction network than previous mechanically mixed electrodes.

The rate performance in the rGO/Si NP microsphere anode LIB was evaluated by measuring the discharge capacity as the current density increased from 1 to 16 A/g, as shown in Fig. 3(c). With a 16-fold increase in current density, the rGO/Si NP microparticles cell maintained a high coulombic efficiency (>99%) while maintaining a reversible capacity of 552 mAh/g. Si microparticles maintained a low capacity of 198 mAh/g under the same conditions (see Fig. S4). This indicates that the capacity retention rate of the cell was 32%. The capacity was restored to 1,539 mAh/g when the current density was returned to 1 A/g after 16 A/g ultra-fast charge/discharge cycling, which shows excellent rate performance. The Nyquist plot of the EIS shows a semicircle due to charge transfer resistance in lithiation (see Fig. 3(d)). A slightly smaller semicircle at higher frequencies is due to the resistance of the SEI film and the charge transfer resistance in lithiation. The rGO/Si NP microsphere anode showed small semicircular than Si microsphere anode. This indicates that conductivity and charge transfer are facilitated by rGO [42].

CONCLUSION

We fabricated Si NPs/rGO microparticles by spray drying of mixed solution of Si NPs and GO and subsequent high temperature heat treatment. Spray drying produces agglomerates of rGO and Si NPs, resulting in a composite of good electrical conductivity. In addition, the spherical particles cause the rGO to crumble and provide pores that can alleviate volumetric changes during charge and discharge. In the LIB application, the rGO/Si NP micro-

sphere anode LIB provided a reversible capacity of 1,246 mAh/g at 1 A/g after 200 charge-discharge cycles. The capacity retention rate after 200 cycles was 83% and the coulombic efficiency was 99%. In contrast, Si-microsphere cells showed a 12% lower capacity maintenance. Also, the rGO/Si NP microsphere anode LIB exhibited high performance rates. As the current density increased from 1 to 16 A/g, the capacity retention was 32%. Our method is simple and easy to scale-up, and can be applied to commercialization of Si/C anode for LIB.

SUPPORTING INFORMATION

Additional information as noted in the text. This information is available via the Internet at http://www.springer.com/chemistry/journal/11814.

REFERENCES

1. P. Poizot, S. Laruelle, S. Grugeon, L. Dupont and J. M. Tarascon, *Nature*, **407**, 496 (2000).
2. M. M. Thackeray, C. Wolverton and E. D. Isaacs, *Energy Environ. Sci.*, **5**, 7854 (2012).
3. N.-S. Choi, Z. Chen, S. A. Freunberger, X. Ji, Y.-K. Sun, K. Amine, G. Yushin, L. F. Nazar, J. Cho and P. G. Bruce, *Angew. Chem. Int. Ed.*, **51**, 9994 (2012).
4. M. Ko, S. Chae, S. Jeong, P. Oh and J. Cho, *ACS Nano*, **8**, 8591 (2014).
5. A. S. Arico, P. Bruce, B. Scrosati, J.-M. Tarascon and W. van Schalkwijk, *Nat. Mater.*, **4**, 366 (2005).
6. A. Manthiram, A. Vadivel Murugan, A. Sarkar and T. Muraliganth, *Energy Environ. Sci.*, **1**, 621 (2008).
7. P. G. Bruce, B. Scrosati and J.-M. Tarascon, *Angew. Chem. Int. Ed.*, **47**, 2930 (2008).
8. S. Choi, D. S. Jung and J. W. Choi, *Nano Lett.*, **14**, 7120 (2014).
9. C. K. Chan, R. N. Patel, M. J. O'Connell, B. A. Korgel and Y. Cui, *ACS Nano*, **4**, 1443 (2010).
10. L. Hu, H. Wu, S. S. Hong, L. Cui, J. R. McDonough, S. Bohy and Y. Cui, *Chem. Commun.*, **47**, 367 (2011).
11. M.-H. Park, M. G. Kim, J. Joo, K. Kim, J. Kim, S. Ahn, Y. Cui and J. Cho, *Nano Lett.*, **9**, 3844 (2009).
12. T. Song, J. Xia, J.-H. Lee, D. H. Lee, M.-S. Kwon, J.-M. Choi, J. Wu, S. K. Doo, H. Chang, W. I. Park, D. S. Zang, H. Kim, Y. Huang, K.-C. Hwang, J. A. Rogers and U. Paik, *Nano Lett.*, **10**, 1710 (2010).
13. T. Zhao, S. She, X. Ji, W. Jin, A. Dang, H. Li, T. Li, S. Shang and Z. Zhou, *J. Alloys Compd.*, **708**, 500 (2017).
14. W.-h. Lee, D.-Y. Kang, J. S. Kim, J. K. Lee and J. H. Moon, *RSC Adv.*, **5**, 17424 (2015).
15. D. Gueon, J. Lee, J. K. Lee and J. H. Moon, *RSC Adv.*, **6**, 38012 (2016).
16. M. Liang and L. Zhi, *J. Mater. Chem.*, **19**, 5871 (2009).
17. T. Zhao, X. Ji, P. Bi, W. Jin, C. Xiong, A. Dang, H. Li, T. Li, S. Shang and Z. Zhou, *Electrochim. Acta*, **230**, 342 (2017).
18. H. Bai, C. Li and G. Shi, *Adv. Mater.*, **23**, 1089 (2011).
19. K. T. Nguyen and Y. Zhao, *Nanoscale*, **6**, 6245 (2014).
20. J. L. Xie, C. X. Guo and C. M. Li, *Energy Environ. Sci.*, **7**, 2559 (2014).
21. Y. Fang, Y. Lv, R. Che, H. Wu, X. Zhang, D. Gu, G. Zheng and D. Zhao, *J. Am. Chem. Soc.*, **135**, 1524 (2013).
22. Y. Zhu, W. Liu, X. Zhang, J. He, J. Chen, Y. Wang and T. Cao, *Langmuir*, **29**, 744 (2013).
23. X. Zhou, Y.-X. Yin, L.-J. Wan and Y.-G. Guo, *Adv. Energy Mater.*, **2**, 1086 (2012).
24. X. Liu, J. Zhang, W. Si, L. Xi, B. Eichler, C. Yan and O. G. Schmidt, *ACS Nano*, **9**, 1198 (2015).
25. X. Gao, J. Li, Y. Xie, D. Guan and C. Yuan, *ACS Appl. Mater. Interfaces*, **7**, 7855 (2015).
26. Y. Chen, F. Guo, Y. Qiu, H. Hu, I. Kulaots, E. Walsh and R. H. Hurt, *ACS Nano*, **7**, 3744 (2013).
27. J. Ma, J. Wang, Y.-S. He, X.-Z. Liao, J. Chen, J.-Z. Wang, T. Yuan and Z.-F. Ma, *J. Mater. Chem. A*, **2**, 9200 (2014).
28. J. Ma, T. Yuan, Y.-S. He, J. Wang, W. Zhang, D. Yang, X.-Z. Liao and Z.-F. Ma, *J. Mater. Chem. A*, **2**, 16925 (2014).
29. Z.-F. Li, H. Zhang, Q. Liu, Y. Liu, L. Stanciu and J. Xie, *ACS Appl. Mater. Interfaces*, **6**, 5996 (2014).
30. J. Luo, X. Zhao, J. Wu, H. D. Jang, H. H. Kung and J. Huang, *J. Phys. Chem. Lett.*, **3**, 1824 (2012).
31. J. Luo, H. D. Jang, T. Sun, L. Xiao, Z. He, A. P. Katsoulidis, M. G. Kanatzidis, J. M. Gibson and J. Huang, *ACS Nano*, **5**, 8943 (2011).
32. D. Shao, D. Tang, Y. Mai and L. Zhang, *J. Mater. Chem. A*, **1**, 15068 (2013).
33. Q. Wu, Y. Xu, Z. Yao, A. Liu and G. Shi, *ACS Nano*, **4**, 1963 (2010).
34. R. M. S. dos Reis, R. L. Maltez, E. C. Moreira, Y. P. Dias and H. Boudinov, *Appl. Surf. Sci.*, **258**, 7395 (2012).
35. H. Yang, Yan, Y. Liu, F. Zhang, R. Zhang, Y. YanMeng, M. Li, S. Xie, B. Tu and D. Zhao, *J. Phys. Chem. B*, **108**, 17320 (2004).
36. H. Tang, J. Zhang, Y. J. Zhang, Q. Q. Xiong, Y. Y. Tong, Y. Li, X. L. Wang, C. D. Gu and J. P. Tu, *J. Power Sources*, **286**, 431 (2015).
37. H. Mi, Y. Li, P. Zhu, X. Chai, L. Sun, H. Zhuo, Q. Zhang, C. He and J. Liu, *J. Mater. Chem. A*, **2**, 11254 (2014).
38. C. Kim, K. S. Yang, M. Kojima, K. Yoshida, Y. J. Kim, Y. A. Kim and M. Endo, *Adv. Funct. Mater.*, **16**, 2393 (2006).
39. H. Jia, P. Gao, J. Yang, J. Wang, Y. Nuli and Z. Yang, *Adv. Energy Mater.*, **1**, 1036 (2011).
40. M. Wang, D. Jia, J. Li and J. Huang, *RSC Adv.*, **4**, 33981 (2014).
41. Q. Xiao, Y. Fan, X. Wang, R. A. Susantyoko and Q. Zhang, *Energy Environ. Sci.*, **7**, 655 (2014).
42. R. Zou, Q. Liu, G. He, M. F. Yuen, K. Xu, J. Hu, I. P. Parkin, C.-S. Lee and W. Zhang, *Adv. Energy Mater.*, **7**, 1601363 (2017).

Supporting Information

Spherical graphene and Si nanoparticle composite particles for high-performance lithium batteries

Jaehyun Lee and Jun Hyuk Moon†

Department of Chemical and Biomolecular Engineering, Sogang University, Seoul 04107, Korea
(*Received 10 March 2017 • accepted 10 August 2017*)

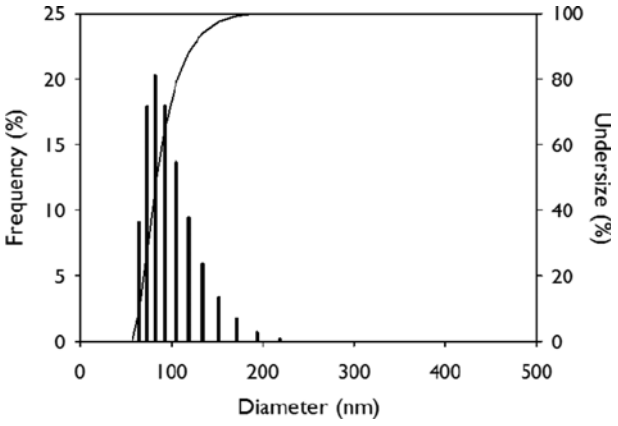

Fig. S1. Size distribution of silicon nanoparticles.

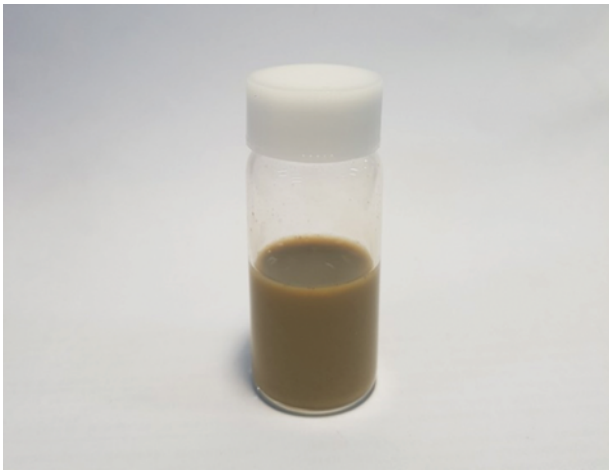

Fig. S2. A photograph of a silicon dispersion that has passed 3 days after preparation.

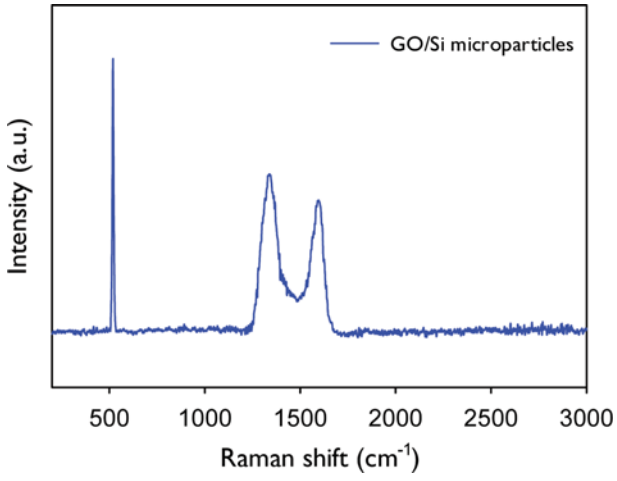

Fig. S3. Raman spectra of GO/Si microparticles.

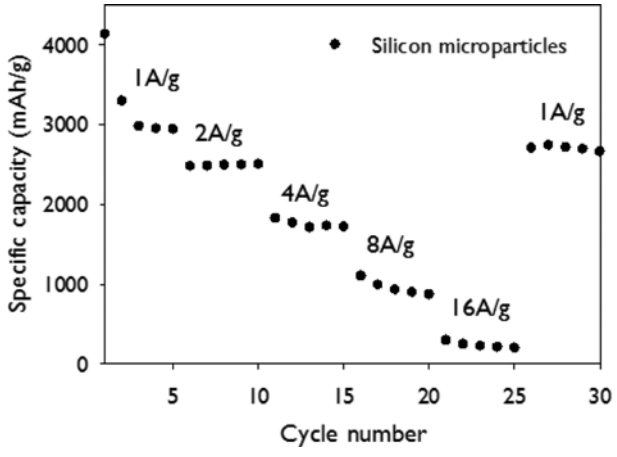

Fig. S4. Rate performance of Si microparticles electrodes measured at various current densities from 1 to 16 A/g.